Selective filtering defect at the axon initial segment in Alzheimer's disease mouse models

Xiaqin Sun[a,1], Yu Wu[a,1], Mingxue Gu[a], Zhuo Liu[a], Yuanlin Ma[b], Jun Li[b], and Yan Zhang[a,2]

[a]State Key Laboratory of Biomembrane and Membrane Biotechnology, College of Life Sciences, PKU-IDG/McGovern Institute for Brain Research, Peking University, Beijing 100871, China; and [b]Peking University Sixth Hospital, Beijing 100191, China

Edited* by Mu-ming Poo, University of California, Berkeley, Berkeley, CA, and approved August 21, 2014 (received for review June 25, 2014)

Axon pathology has been widely reported in Alzheimer's disease (AD) patients and AD mouse models. Herein we report that increased miR-342–5p down-regulates the expression of ankyrin G (AnkG), a protein known to play a critical role in establishing selective filtering machinery at the axon initial segment (AIS). Diminished AnkG expression leads to defective AIS filtering in cultured hippocampal neurons from AD mouse models, as monitored by selective exclusion of large macromolecules from the axons. Furthermore, AnkG-deficiency impairs AIS localization of Na_v 1.6 channels and confines NR2B to the somatodendritic compartments. The expression of exogenous AnkG improved the cognitive performance of 12-mo-old APP/PS1 mice; thus, our data suggest that AnkG and impairment of AIS filtering may play important roles in AD pathology.

Alzheimer's disease (AD), the most common cause of dementia in individuals age >65 y, is associated with impairments in memory, language, behavior, and cognition (1). The brain of AD patients is characterized by extracellular senile plaques composed of amyloid β (Aβ), intracellular tau aggregates known as neurofibrillary tangles, and neuronal loss (1). Axonal pathology, including axonal swellings and abnormal accumulation of axonal proteins, is associated with dystrophic neurites and amyloid plaque formation in AD (2). Abundant age-dependent axonal spheroids and myelin ovoids have been reported in the spinal cord of $APP_{Swe/London}/PS1_{M146V}$ mice, an established familial form of AD (FAD) transgenic mouse model (3); however, the cause of the axonopathy and the pathways involved in axonal abnormalities in AD remain largely unknown.

MicroRNAs (miRNAs) are a class of conserved, short, noncoding RNAs (4–8), many of which have demonstrated implications in AD (9–11). We have previously reported that miR-342–5p is up-regulated in APP/PS1, PS1ΔE9, and PS1-M146V transgenic AD mice, which is mechanistically linked to elevated β-catenin, c-Myc, and IFN regulatory factor (IRF)-9 (12). MiRNAs interact with the 3′ UTR or 5′ UTR region of complementary mRNA sequences (13), inducing translation repression or target degradation (14, 15). In previous work, we demonstrated that increased miR-342–5p down-regulates the expression of ankyrin G (AnkG) (12), a protein known to play a critical role at the axon initial segment (AIS).

The AIS is known to play an important role in neuronal polarity formation, action potential initiation (16, 17), and brain diseases and injury (18). At the AIS, a plasma membrane barrier segregates the axonal from the somatodendritic membrane compartments (19), and a filtering machinery sorts cytoplasmic components that are destined for transport into the axon (19, 20). In cultured embryonic rat hippocampal neurons at embryonic day (E) 18, a selective filter develops at 5 d in vitro (DIV; 2 d after axon/dendrite differentiation), with an average pore size of ≤13 nm (20). This physical barrier may represent a high-density meshwork at the AIS composed of actin and AnkG. AnkG has been demonstrated to play an important role in maintaining the structure of AIS and in the generation/maintenance of neuronal polarity (21–24). This filtering machinery is critical for selective transport of macromolecules into the axon; for example, KIF5-driven carriers of the synaptic vesicle protein VAMP2, but not KIF17-driven carriers of dendrite-targeting NMDA receptor subunit NR2B, can enter the axon (20). Thus, selective filtering at the AIS is suggested to contribute to preferential trafficking and segregation of cellular components in polarized neurons (20).

Herein we report that in APP/PS1, PS1ΔE9, and PS1-M146V mouse hippocampal neurons, down-regulation of AnkG by miR-342–5p results in impairment of selective filtering at the AIS in these AD transgenic mouse neurons, and that ectopic expression of AnkG reverses AIS filtering abnormalities. The deficits of the filtering machinery in the AIS of APP/PS1 mice lead to mislocation of the Na_v 1.6 channels and the NR2B. Taken together, our results point to an aberrant AnkG-defective AIS filtering mechanism as a critical determinant of axonal and neuronal pathology in AD mouse models.

Results

AIS Selective Filtering Was Impaired in AD Transgenic Mouse Neurons. In WT and APP/PS1 neurons, the axons and dendrites were distinguished by immunostaining with the specific axonal marker Tau-1 and the dendritic marker MAP2 (Fig. 1 *A* and *B* and Fig. S1). MAP2 distinctively stained the soma and dendrite, with no overlap staining of the axon (Ax) (Fig. 1 *A* and *B* and Fig. S1). However, Tau-1 staining partially colocalized with MAP2 labeling in some of the dendrites (arrowhead), particularly in APP/PS1 neurons (Fig. 1*A* and Fig. S1). Therefore, we decided to use the absence of MAP2 staining instead of Tau-1 labeling to identify the axon.

To investigate the integrity of the filtering machinery at the AIS in APP/PS1 mice, we microinjected 10-kDa and 70-kDa dextran into the soma of hippocampal neurons cultured for 7 DIV from E14 embryos, and used MAP2 staining as a soma-dendritic

Significance

It is widely accepted that Alzheimer's disease (AD) is an age-related disease that is always associated with later stages of life. However, our data indicates that if carrying familial AD mutations (such as the PS1 mutations examined in this study), neurons are perturbed during development, protein trafficking, protein translocation, and axon initial segment (AIS) subcellular structure formation. Given that AIS is associated with action potential generation and NR2B is highly related to synaptic transmission, we think that this may subsequently lead to many problems associated with misfiring and synaptic transmission in these AD neurons, and may further contribute to AD development and pathology.

Author contributions: Y.Z. designed research; X.S., Y.W., M.G., Z.L., Y.M., and J.L. performed research; X.S., Y.W., M.G., Y.M., J.L., and Y.Z. analyzed data; and Y.Z. wrote the paper.

The authors declare no conflict of interest.

*This Direct Submission article had a prearranged editor.

[1]X.S. and Y.W. contributed equally to this work.

[2]To whom correspondence should be addressed. Email: yanzhang@pku.edu.cn.

This article contains supporting information online at www.pnas.org/lookup/suppl/doi:10.1073/pnas.1411837111/-/DCSupplemental.

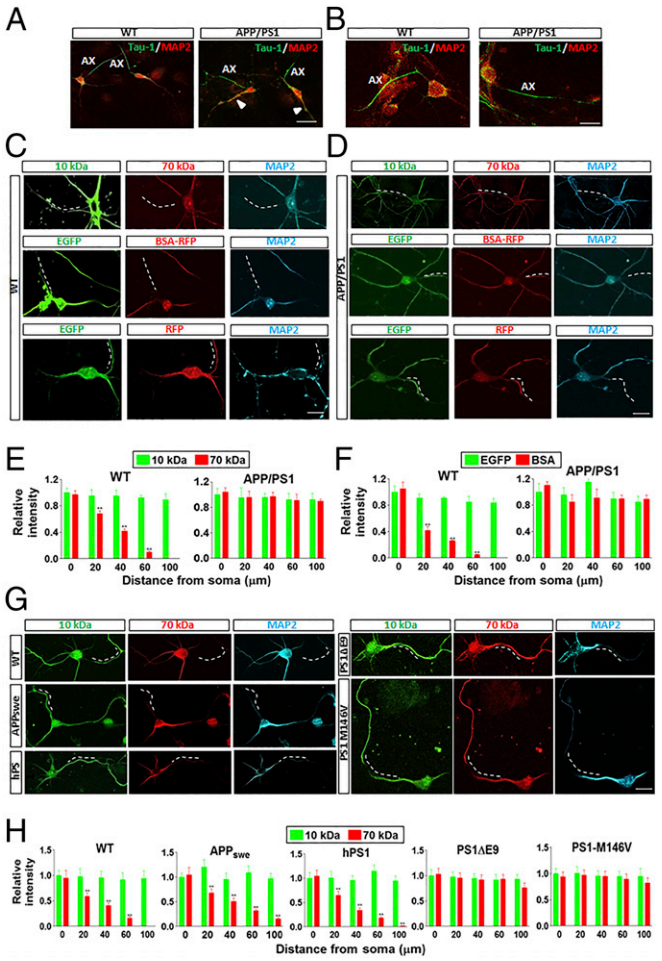

Fig. 1. APP/PS1 mouse neurons have impaired filtering machinery at the AIS. (*A*) WT and APP/PS1 neurons were stained by Tau-1 (red) and MAP2 (green). MAP2 specifically labeled the soma and dendrites. Tau-1 labeled the axons (Ax), with overlap with MAP2 staining in some of the dendrites (arrowhead). (Scale bar: 50 μm.) (*B*) High-power images of the WT and APP/PS1 neurons stained with Tau-1 and MAP2. (Scale bar: 10 μm.) (*C* and *D*) Examples of axonal diffusion of 10-kDa and 70-kDa dextran, EGFP (~27 kDa), and BSA-RFP (~90 kDa) loaded in the soma of WT or APP/PS1 mouse hippocampal neurons at 7 d in vitro (DIV). The dashed line represents the AIS. (Scale bar: 10 μm.) (*E* and *F*) Summary of the data for 10-kDa and 70-kDa dextran-, EGFP-, and BSA-RFP–positive areas in the axons of WT or APP/PS1 mouse neurons. (*G*) Examples of axonal diffusion of 10-kDa and 70-kDa dextran loaded in the soma of WT, APP/PS1, hPS1, PS1ΔE9, and PS1-M146V mouse hippocampal neurons at 7 DIV. The dashed line represents the AIS. (Scale bar: 10 μm.) (*H*) Summary of the data for 10-kDa and 70-kDa dextran-positive areas in the axons of neurons in various transgenic lines. Data are mean ± SE ($n = 10$ for each group). $^{**}P < 0.01$ compared with 10-kDa dextran.

marker. In WT mouse neurons, the smaller 10-kDa dextran diffused into the axon, whereas the larger 70- kDa dextran failed to do so, suggesting the presence of a selective cytoplasmic filter at 7 DIV, similar to that reported previously for 5 DIV hippocampal neurons (20) (Fig. 1*C*). Furthermore, microinjected EGFP (~27 kDa) could diffuse into the axon, whereas RFP-conjugated bovine serum albumin (BSA) (BSA-RFP; ~90 kDa) could not (Fig. 1*C*). However, in APP/PS1 mouse neurons, both small (10-kDa dextran and EGFP) and large macromolecules (70-kDa dextran and BSA-RFP) macromolecules diffused into the axon, indicating impaired filtering machinery (Fig. 1*D*). Loaded EGFP (~27 kDa) and RFP (~27 kDa) penetrated into the axons of both WT and APP/PS1 mouse neurons (Fig. 1 *C* and *D*). These results demonstrate that macromolecular penetration into the axon has a size limit in WT neurons (Fig. 1 *E* and *F*), further corroborating the existence of a selective filter at the AIS, which is impaired in APP/PS1 mice.

Because APP/PS1 mice harbor transgenes encoding the FAD-linked APPswe and PS1ΔE9 polypeptides, we sought to examine changes in the selective filtering in transgenic mice by expressing the genes individually (APPswe, human WT PS1, or PS1ΔE9), together with an independent transgenic line expressing the FAD-linked M146V variant. Interestingly, neurons from all PS1 mutant lines demonstrated severely impaired AIS filtering compared with hWTPS1 and the APPswe mutant line (Fig. 1 *G* and *H*).

Average lateral diffusion coefficient (D) values were measured at the AIS by microinjecting neurons with quantum dots (QDs) at the soma and capturing the live images of QD movement (Fig. S2*A*). Our data demonstrate that at the AIS, in neurons cultured from both E15 and newborn mice, APP/PS1 neurons exhibited significantly greater lateral movement of QDs than WT neurons, and this movement can be partially reversed by AnkG injection (Fig. S2 *B* and *C*). This further suggests that the impaired filtering at the AIS of APP/PS1 neurons might affect protein diffusion and trafficking in the axon.

In the early stages, the development of APP/PS1 neurons was markedly slower than that of WT neurons. To exclude the possibility that the selective filter had not fully developed at 7 DIV in the APP/PS1 mice, we performed similar molecular tracing experiments on 10-kDa and 70-kDa dextran in hippocampal neurons cultured from newborn APP/PS1 mice for 5 DIV (Fig. S3*A*) and from E14 embryos for 14 DIV (Fig. S3*B*). Our data demonstrate that the 70-kDa dextran could diffuse into the axon in both cases, suggesting that the impairment of selective filtering at the AIS is not related to delayed development.

MiR-342–5p and AnkG Rescued Impaired AIS Filtering in AD Neurons. Given that AnkG is a target of miR-342–5p, and that down-regulation of AnkG in mutant mice could occur at the level of protein translation (12), we further tested the role of miR-342–5p in regulating AIS filtering. We found that microinjections of miR-342–5p into the cultured WT neurons significantly reduced the level of AnkG at the AIS (Fig. 2 *A* and *C*). Furthermore, microinjections of miR-342–5p and its mimics resulted in impaired AIS filtering in WT neurons similar to that seen in APP/PS1 neurons (Fig. 2 *B* and *D*). In contrast, microinjections of the inhibitor of miR-342–5p into APP/PS1 neurons prevented the impairment of AIS filtering (Fig. 2 *B* and *D*). In APP/PS1 neurons, comicroinjections of AnkG-expressing construct with its 3′ UTR and miR-342–5p or its mimics produced no rescue of filtering impairment by the exogenous AnkG (Fig. 2*D*). However, when the construct expressing AnkG without its 3′ UTR was comicroinjected with miR-342–5p or its mimics, expression of exogenous AnkG could still restore AIS filtering because of ineffective regulation of miR-342–5p (Fig. 2*D*).

We found that in APP/PS1 mouse neurons, exogenous expression of microinjected AnkG constructs (25) reestablished the selective filter function (Fig. 2 *E* and *F*), suggesting that AnkG deficits contribute to impaired integrity of the selective filter at the AIS in APP/PS1 mice. In contrast, microinjections of only a control vector or the mutant AnkG (A1024P) lacking the spectrin-binding domain (25) did not restore the filtering machinery in APP/PS1 mouse neurons (Fig. 2 *E* and *F*). Moreover, expression of AnkG could prevent the impairment of AIS filtering in PS1ΔE9 and PS1-M146V neurons, whereas expression of AnkG-A1024P had no effect (Fig. 2 *E* and *F*).

Impaired AIS Filtering May Underlie Functional Defects in APP/PS1 Mice. Previous studies have shown that AnkG is responsible for the recruitment of neurofascin, βIV spectrin, and Na^+ channels to the AIS (26–29). Western blot analysis of the levels of these proteins in hippocampal tissues demonstrated a ~50% lower neurofascin level in APP/PS1 mice compared with WT mice.

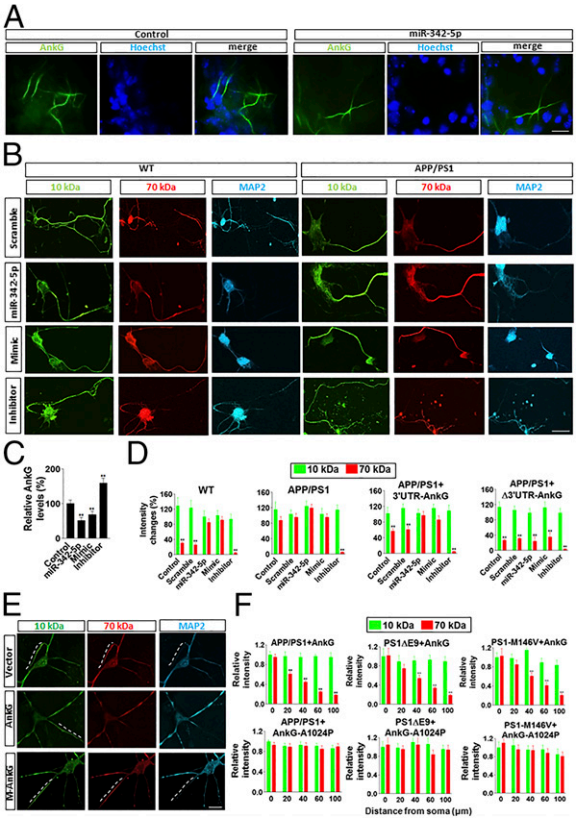

Fig. 2. MiR-342–5p and AnkG rescued the impaired filtering in the AIS of APP/PS1 neurons. (*A* and *C*) In WT neurons, overexpression of miR-342–5p by microinjection reduced AnkG expression markedly. MiR-342–5p expression was calculated by the number of AnkG-positive (green) over 100 cells (Hoechst). (*B* and *D*) In WT neurons, microinjection of miR-342–5p or mimics of miR-342–5p induced impaired AIS filtering. In APP/PS1 neurons, the inhibitor of miR-342–5p rescued impaired AIS filtering. (Scale bar: 10 μm.) The intensity was measured at 80 μm from the soma along the axon. In APP/PS1 neurons, comicroinjection of the construct expressing AnkG and its 3′ UTR sequence with scramble miRNA or I-miR-342–5p (inhibitor of miR-342–5p) reduced or prevented the impairment of AIS filtering, but that with miR-342–5p or M-miR-342–5p (mimics of miR-342–5p) did not. When the construct expressing the mutant AnkG with the deletion of the 3′ UTR responsive region for miR-342–5p was comicroinjected with miR-342–5p or its mimics, AIS filtering impairment was prevented. Data are mean ± SE ($n = 10$ for each group). $^{**}P < 0.01$ compared with 10-kDa dextran. (*E*) Exogenous expression of AnkG, but not of the mutant AnkG-A1024P, reversed the impaired AIS filtering machinery in APP/PS1, PS1ΔE9, and PS1-M146V mouse neurons. (*F*) Quantification of the data. The dashed line represents the AIS. Data are mean ± SE ($n = 10$ for each group). $^{**}P < 0.01$ compared with WT. (Scale bar: 10 μm.)

There was no significant difference in the levels of βIV spectrin and the Na^+ channel between the two groups of mice (Fig. 3*A*). In the AIS, Na^+ channel 1.6 (Na_v 1.6) is known to be critical for action potential initiation (30). We found that Na_v 1.6 colocalized mostly with AnkG at the AIS in WT neurons, whereas Na_v 1.6 was distributed along the entire axon and lower levels were detected in the AIS region of APP/PS1 neurons (Fig. 3*B*).

The normal dendritic distribution of glutamate receptors is critical for neuronal function. The 2B subunit of the NMDA subtype of glutamate receptors (NR2B) is known to be located at the soma and dendrite of these cultured hippocampal neurons, owing to selective transport mediated by the kinesin superfamily of proteins (20, 31, 32). We found that in WT mouse neurons at 7 DIV, NR2B was located exclusively at the soma and dendrite, as reported previously (20), whereas in APP/PS1 mouse neurons, NR2B was transported into the axon (Fig. 3 *C* and *D*), possibly owing to the impaired filtering machinery. Microinjection of the construct expressing AnkG into APP/PS1 mouse neurons led to a normal distribution of NR2B in the soma-dendritic compartment (Fig. 3 *C* and *D*). In contrast, expression of the mutant AnkG-A1024P did not rescue the phenotype (Fig. 3 *C* and *D*). In contrast, in WT neurons, AnkG siRNA induced impairment of AIS filtering (Fig. 3*E*). Our in vivo data indicate that in the hippocampal tissues from 3 mo-old WT and APP/PS1 mice, the colocalization of AnkG and NR2B at the AIS region is more significant in the APP/PS1 mouse tissue than in the WT tissue (Fig. S4).

To verify that AnkG rescued the AIS filtering impairment in APP/PS1 mouse brain tissue in vivo, we applied in utero electroporation to overexpressing EGFP-fused AnkG (AnkG-EGFP) into the layer II-IV of cortex of E14.5 embryos. These electroporated embryos were then returned and left to develop to postnatal day (P) 0. The APP/PS1 neurons showed more NR2B axonal localization than the WT neurons (Fig. 3*F*). With overexpression of AnkG, the number of neurons with axonal localized NR2B decreased dramatically, suggesting that AnkG can rescue the AIS filtering impairment in APP/PS1 mouse brain tissue in vivo (Fig. 3*F*). MiR-342–5p, its inhibitor, or scramble control miRNA was

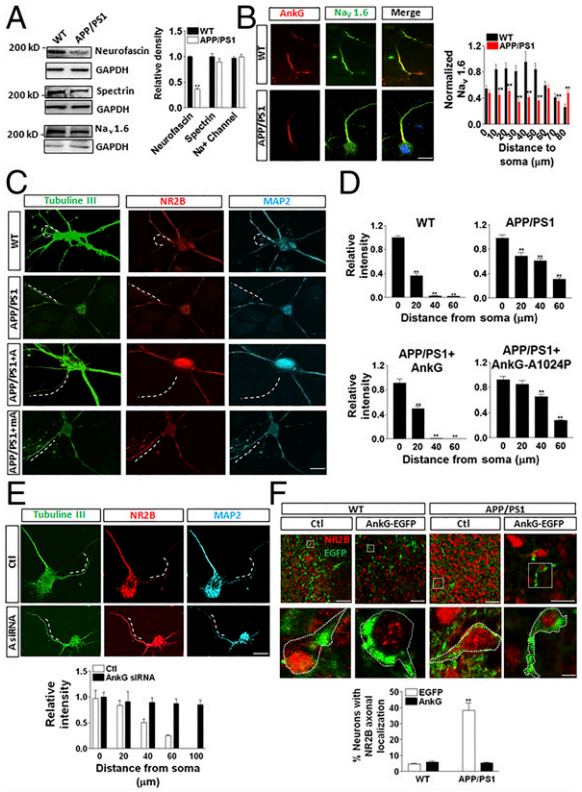

Fig. 3. Impaired AIS filtering might underlie functional defects in APP/PS1 neurons. (*A*) In APP/PS1 neurons, the levels of neurofascin, but not of spectrin or Na_v 1.6, were decreased significantly. (*B*) In WT neurons, Na_v 1.6 aggregated to the AIS region, whereas in APP/PS1 neurons, Na_v 1.6 distributed along the entire axon. (Scale bar: 20 μm.) (*C* and *D*) In WT mouse neurons, NR2B was located mainly at the soma and dendrites, whereas in APP/PS1 mouse neurons, NR2B was abnormally located on the axon. AnkG reversed the impaired NR2B location in APP/PS1 mouse neurons. The dashed line represents the AIS. (Scale bar: 10 μm.) (*E*) AnkG siRNA (A siRNA) induced the impairment of AIS filtering in WT neurons. Red, NR2B; green, AnkG fused with EGFP. (Scale bar: 20 μm.) (*F*) An in utero electroporation experiment showed that exogenous AnkG rescued the mislocation of NR2B in the axon in APP/PS1 neurons. Data are mean ± SE ($n = 10$ for each group). $^{**}P < 0.01$ compared with control. (Scale bars: *Upper*, 100 μm; *Lower*, 5 μm.)

transduced into cortical layers II–IV of E14.5 WT mouse embryos by in utero electroporation with cytomegalovirus early enhancer/chicken β-actin promoter-driven EGFP. The data show that in WT neurons, miR-342–5p induced colocalization of NR2B with AnkG in the axon, whereas inhibitor or scramble did not (Fig. S5).

To evaluate whether AIS function affects axon maintenance, we measured the number of axons per neuron at 5 DIV and 14 DIV. Our data show that at both 5 DIV and 14 DIV, APP/PS1 neurons had roughly the same number of axons per neuron as WT neurons (Fig. 4*A*). At 21 DIV, AnkG staining revealed no difference in the number of axons per neuron between WT and APP/PS1 neurons (Fig. 4*B*), suggesting that the AIS function does not affect axonal maintenance; however, the average axon length was significantly shorter in the APP/PS1 neurons compared with the WT neurons at 14 DIV (Fig. 4*C*).

Because the AIS filtering changed the localization of synaptic proteins, such as NR2B, we also investigated the formation of synapses. Our data demonstrate that after labeling with the presynaptic marker synapsin, both the number and size of synapses were significantly lower in APP/PS1 neurons than in WT neurons (Fig. 4*D*), implying possible defects in synapse formation and plasticity.

To verify the rescue of AIS filtering function in both 12-mo-old and 18 mo-old animals, adenovirus packaging AnkG-EGFP and NR2B-RFP was used to infect the CA1 region of the hippocampus of 12-mo-old and 18 mo-old APP/PS1 mice (Fig. S6). In both the 12-mo-old and 18-mo-old APP/PS1 mouse CA1 tissues, exogenous overexpression of AnkG decreased the colocalization of NR2B and AnkG in the AIS and axon regions (Fig. S6), implying that AnkG could rescue the AIS filtering function at both 12 and 18 mo of age.

We evaluated spatial learning and memory using the Morris water maze test in 12-mo-old and 18-mo-old WT and APP/PS1 mice. At both ages, APP/PS1 mice exhibited significant cognitive defects, indicated by the latency of the findings from the platform and probe test, compared with WT mice (Fig. 4*E*). We found that infecting the CA1 area of the hippocampus of APP/PS1 mice with the adenovirus containing the AnkG construct greatly improved cognitive performance in APP/PS1 mice at age 12 mo (Fig. 4*E*), indicating that AnkG expression and AIS filtering in neurons may affect learning and memory. In addition, there appeared to be a critical window during which AnkG could rescue the cognitive impairment, because overexpression of AnkG did not improve the animal's overall performance in the water maze at age 18 mo.

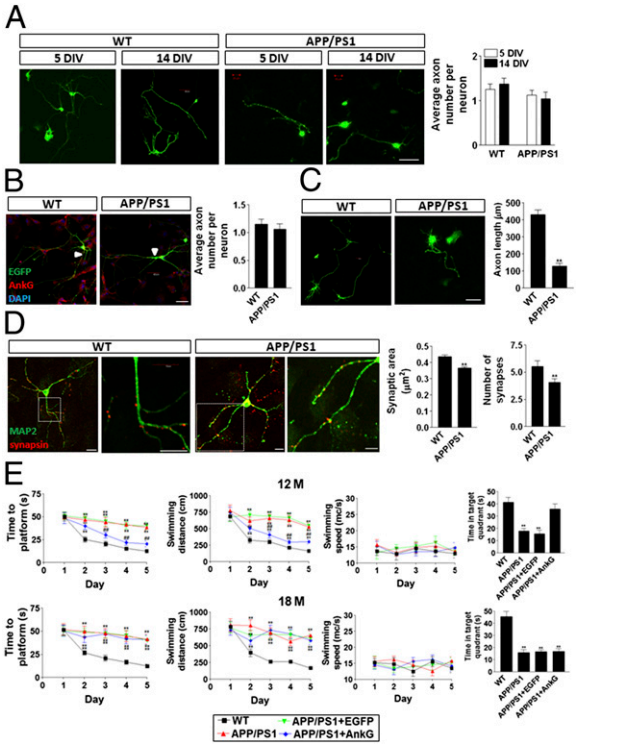

Fig. 4. Impaired AIS filtering induced axonal, synaptic, and cognitive defects in APP/PS1 neurons and mice. (*A*) No difference was detected in the number of axons per neuron in 5 DIV and 14 DIV WT and APP/PS1 neurons. (Scale bar: 20 μm.) (*B*) No difference was detected in the number of axons per neuron in 21 DIV WT and APP/PS1 neurons. EGFP (green) was randomly transfected into neurons, and AnkG (red) was stained by its antibody. The arrow indicates the AIS. (Scale bar: 20 μm.) (*C*) The axons of the WT neurons were significantly longer than those of the APP/PS1 neurons at 14 DIV. (Scale bar: 20 μm.) (*D*) The number of synapses and overall synaptic area were remarkably larger in WT neurons than in APP/PS1 neurons at 14 DIV. Data are mean ± SE ($n = 10$ for each group). $^{**}P < 0.01$ compared with WT. (Scale bar: 20 μm.) (*E*) The AnkG construct was packaged into adenovirus and infected in the hippocampal CA1 region of APP/PS1 mice. Overexpression of AnkG significantly improved Morris water maze spatial learning and memory performance in 12-mo-old, but not in 18-mo-old, APP/PS1 mice. Data are mean ± SE ($n = 8$ for each group). $^{\#\#}P < 0.01$ compared with APP/PS1 or control; $^{**}P < 0.01$ compared with WT.

Discussion

In the present study, we found that decreasing AnkG levels by up-regulation of miR-342–5p contributes to the impairment of selective filtering at the AIS in AD transgenic mice, including APP/PS1, PS1ΔE9, and PS1-M146V lines. Therefore, in AD transgenic mouse neurons, down-regulated AnkG leads to the disruption of the AIS filtering, which in turn could cause dysfunction of protein trafficking and protein localization (Fig. S7).

The presence of a selective filter at the AIS has been examined using various approaches. With neurons directly frozen, freeze-substituted, and critical point-dried, a well-preserved filamentous meshwork and a cytoplasmic ground substance were observed in the *Drosophila* axoplasm (33). Electron microscopy revealed that at the AIS, microtubules are of high density and subsequently form fascicles, different from the homogeneous distribution of microtubules at the dendrite (34). Consistent with Song et al. (20), we found that the presence of a selective filter at the AIS early in development (7 DIV) prevents the axonal entry of large macromolecules and vesicular cargos carrying NR2B. Interestingly, one AD model animal, APP/PS1 mice, had a dysfunctional filter at the AIS, which may lead to axonal transport defects of certain synaptic proteins and in turn induce synaptic dysfunction. AIS is critical for action potential initiation, because Na_v 1.6 channels clusters around this area (16, 17, 29, 30). We also found that Na_v 1.6 and NR2B are mislocated in APP/PS1, PS1ΔE9, and PS1-M146V neurons. Our conclusions are consistent with the observation that neuronal excitability and synaptic transmission are affected in these animals (35–38). Remarkably, in the FAD patients associated with PS1, cerebellar dysfunction, including ataxia, Purkinje cell simple spike activity, and mitochondrial transport, occurs before the appearance of Aβ deposition (39).

Some proteins associated with axonopathy, such as neuronal pentraxin 1 (NP1), a protein involved in excitatory synapse remodeling, are elevated in cell processes in the cerebral cortex and hippcampus of APP/PS1 mice (40). Interestingly, NP1 is elevated in dystrophic neurites in the brain tissues of AD patients and colocalizes with tau, suggesting that NP1 is related to axon abnormality (40). At 4 mo of age, APP/PS1 mice develop degenerative changes in serotonin-containing axons innervating the dentate gyrus of the hippocampus (41). Our present results indicate that APP/PS1 mice have impaired selective filtering machinery at the AIS, which leads to abnormal axonal targeting. In

PS1 mutant mice (PS1ΔE9 and PS1-M146V), impaired rapid axonal transport has been reported (42). It is possible that AIS filtering is impaired in APP/PS1 and PS1 mutant mice, resulting in abnormal trafficking of proteins, which may induce protein aggregation in the axon, leading to abnormal axonal rapid transport. This may contribute to axonopathy observed in AD and other neurodegenerative diseases.

Finally, although AD has been considered an aging-associated disorder, our data demonstrate that developmental defects, including AIS filtering, protein trafficking, and localization, can be observed at very early stages in AD transgenic model mice. This is consistent with the finding that the protein expression profile from the presymptomatic PS1 mutation carriers differs significantly from that of age-matched noncarriers (43). Greater cortical florbetapir binding on PET analysis has been reported in asymptomatic PS1 mutation carriers compared with age-matched noncarriers at approximately 20 y before the predicted median age of onset of mild cognitive impairment (44). Our data suggest the possible involvement of neuronal development in the pathogenesis of AD.

Experimental Procedures

Cell Culture. Primary neurons were cultured from E14, E15, and newborn WT, APP/PS1 (APPswe/PS1ΔE9; human APP Swedish mutant/human PS1 exon 9 deletion), APPswe, WT human PS1 knock-in (hPS1), PS1ΔE9, and PS1-M146V mouse hippocampus, following the rules and regulations of Peking University Animal Care and Use Committee as described previously (45). In brief, the fresh hippocampal tissues were dissociated with 0.25% trypsin (Life Technologies), which was then inactivated by 10% decomplemented FBS (HyClone). The mixture was titrated through a pipette to make a homogenous mixture. After filtering through a 70-μm sterilized filter, the flow-through was centrifuged. The pellet was then washed once with PBS (0.14 M NaCl, 0.003 M KCl, 0.01 M Na_2HPO_4, and 0.002 M KH_2PO_4, pH 7.2) and once with DMEM in Earle's balanced salt solution containing 0.225% sodium bicarbonate, 1 mM sodium pyruvate, 2 mM L-glutamine, 0.1% dextrose, and 1× Pen Strep (all from Life Technologies) with 5% FBS. Cells were then plated on poly-L-lysine (Sigma-Aldrich)-coated plates or glass coverslips at a density of 5×10^4 cells/mL Neurons were incubated at 37 °C in DMEM without phenol red with 5% FBS and with 5% circulating CO_2. Cytarabine was added to the culture medium at 24 h after plating at a concentration of 10 μM to inhibit dividing cell growth. The medium was changed every 48 h. SH-Sy5y cells were cultured with MEM (Life Technologies) (45).

Microinjection. Thin-walled borosilicate glass capillaries (outer diameter, 1.0 mm; inner diameter, 0.5 mm) with a microfilament (MTW100F-4; World Precision Instrument) were pulled with a Flaming/Brown Micropipette Puller (P-97; Sutter) to obtain injection needles with a tip diameter of ∼0.5 μm. Microinjections were performed in the cytosol of each cell using and Eppendorf FemtoJet microinjector and micromanipulator. Neurons were injected into the soma areas at 25 fl/shot at an injection pressure of 100 hPa, a compensation pressure of 50 hPa, and an injection time of 0.1 s. Dextran Texas red was diluted with PBS and centrifuged to remove aggregates before being microinjected at 10 mg/mL (20). EGFP (Molecular Probes) and RFP-BSA were injected at 100 μg/mL QD (Jiayuan Quantum Dots Co.; 10 nm diameter) was injected at 100 μg/mL. AnkG and AnkG-A1024P (a kind gift from Dr. V. Bennett, Duke University) (25) were subcloned into pCDNA3.1 or pEYFP-C1 to created fusion proteins of AnkG and EYFP. The constructs were injected at 30 μg/mL (45).

Sources of Reagents and Sequences of miRNAs. Dextrans (10 and 70 kDa) were purchased from Molecular Probes. Mouse miR-342–5p, scramble miRNA control, mimic miR-342–5p, miR-342–5p inhibitor, and mutant miR-342–5p (5′-AGGGACACUAUCUGUGAUUGAG-3′), reversed miR-342–5p (5′-GAGUUAGUGUCUAUCGUGGGGA-3′), and complementary sequence (5′-AGGGUGCCUAU-3′) were purchased from Qiagen (12). MiRNAs were transfected into SH-Sy5y cells with HiPerFect Transfection Agent (Qiagen) or microinjected into primary neurons. All AnkG siRNAs (Qiagen) were diluted into 5 nM before injection, as recommended by the manufacturer. The silencing efficiency and off-target effects of all siRNAs were verified by Qiagen.

Western Blot Analysis. Neuronal proteins were extracted in the cell lysis buffer (50 mM Tris pH 8.0, 150 mM NaCl, 1% Nonidet P-40, and 0.1% SDS), and protein concentrations were measured by the bicinchoninic acid (BCA) assay (Pierce). Protein extracts were denatured at 100 °C for 5 min and separated on 15% SDS/PAGE at 70 V for ∼2 h. Proteins were transferred to Immobilon-P PVDF membrane (Millipore) at 100 mA for 2 h. The membrane was blocked with 5% nonfat milk in Tris-buffered saline with 0.1% Tween 20 (TBS-T) at room temperature for 1 h. Anti-AnkG (4G3F8; Life Technologies), neurofascin (Abcam), βIV spectrin (Abcam), Na^+ channel (Abcam), and GAPDH (Sigma-Aldrich) antibodies were diluted at 1:1,000 for Western blot analyses as primary antibodies. After three washes of 10 min each with TBS-T, HRP-conjugated goat anti-rabbit or anti-mouse IgG was added at a dilution of 1:2,500 as the secondary antibody. The secondary HRP was detected by enhanced chemiluminescence. Optical density was analyzed by BioRad ChemiDox (BioRad). The relative density was calculated using the total absolute density of the target band/loading control (45).

Immunostaining. Cells were permeablized in PBS-Triton at 4 °C and blocked with 10% donkey serum at room temperature, followed by incubation with anti-AnkG antibody (4G3F8; Life Technologies, 1:200), MAP2 (Abcam), tubulin (Sigma-Aldrich), synapsin (Cell Signaling), or NR2B (Sigma-Aldrich; 1:1,000) at 4 °C for 24 h. Cy2- or Cy3-conjugated donkey anti-rabbit antibodies and AMCA-conjugated goat anti-chicken antibody were applied as the secondary antibody. The nuclei were then stained with Hoechst 33258 (1 μg/mL; Sigma-Aldrich) for 15 min in the dark. The coverslips were mounted with Immunon mounting medium (Shandon) onto glass slides, and analysis was performed with a laser confocal fluorescence microscope (Leica TCS SP5). Images were acquired under a 63×/1.4 numerical aperture lens.

Fluorescence Imaging and Analysis of QD. A Nikon Super-Resolution *N*-SIM microscope was used to analyze the high-resolution data. Each image was collected using a 100× oil-immersion objective. The average fluorescence intensities were measured at various distances from the soma area using NIS-Ements AR software (Nikon). To quantify the data, 15 frames were averaged, after subtraction of background fluorescence intensity. To measure the QD diffusion coefficient, QDs were loaded into the neuronal soma by microinjection. The traces of QD movement were recorded with 500 consecutive frames. The movements were then analyzed by Imaging Pro Software to calculate as $D = x^2/2t$, where t is the specific time point and x is the distance from QD to the origin.

Adenovirus Infection. AnkG-EGFP and NR2B-RFP cDNA were subcloned from pEGFP-N3 into pAdTrack with BglII and XhoI digestion. Adenovirus was packaged in HEK293 cells, and the infectious particle was measured as 2×10^6/mL (multiplicity of infection = 1.33). To infect the cell cultures, the purified virus supernatant was added to the cell culture medium at a 1:500 dilution for 24 h.

Morris Water Maze. ***Animal treatments.*** Male WT and APP/PS1 mice (body weight ∼30 g) were used in the water maze experiments. Mice were housed under constant temperature and humidity conditions on a 12-h light/12-h dark cycle with food and water available. Mice were divided into four groups: WT, APP/PS1, APP/PS1 with EGFP (1 μL of EGFP-expressing virus), and APP/PS1 with AnkG (1 μL of AnkG-expressing virus). The solution was injected into each hippocampal CA1 over a 2-min period through a Hamilton microsyringe, and the needle was left in place for additional 3 min. The injections were performed for 3 consecutive days.

Water maze tests. The Morris water maze apparatus consisted of a circular swimming pool measuring 60 cm in radius and 50 cm high placed in a room with numerous extramaze cues available on the walls. The pool was filled to a depth of 30 cm with 21–22 °C water. The hidden platform top was a circular plate measuring 10 cm in diameter. The hidden platform was located 2 cm below the water surface. The next day, mice were trained to escape onto the hidden platform in the water maze. The pool was conceptually divided into four quadrants of equal area. The hidden platform was placed in the center of one quadrant throughout the experiment. Each of the four cardinal points of the perimeter of the pool was used at random as a starting location. Before the experiment, the time that the mouse spent in each quadrant (including the target quadrant) without the platform was recorded. A trial began when a mouse was placed in the pool facing the wall and ended when the rat escaped onto the platform. The escape latency to the platform was recorded. If a rat failed to escape within 60 s, then the trial was terminated and the escape latency was defined as 60 s, and the mouse was guided to the platform by the experimenter. The mice were subjected to four trials per day for 5 consecutive days (for a total of 20 trials). A probe trial test was carried out on the sixth day, by recording the times spent in each quadrant without a platform (45).

In utero electroporation. Mother mice carrying embryos at E14.5 were anesthetized with 0.7% Nembutal, and surgery was performed as described previously (46). The DNA plasmid at a concentration of 2.5 μg/μL diluted in PBS was injected to lateral ventricles of embryos by a micropipette with a total amount of 2 μL. The electroporator (NEPA21 Super Electroporator; Nepa Gene) was set at five square pulses of 10 V for 50 ms at 50-ms intervals for eletroporation. With the uterus placed back to the abdominal cavity, the embryos could recover and develop. The follow-up experiments were performed at P0.

Statistical Analysis. Statistical significance was assessed by one-way ANOVA. The Sheffé test was applied as a post hoc test for the significant difference revealed by ANOVA. A P value < 0.05 was considered to indicate statistical significance.

ACKNOWLEDGMENTS. We thank Dr. Sangram Sisodia (University of Chicago), Dr. Vann Bennett (Duke University), and Dr. Dai Zhang (Peking University Sixth Hospital) for their inspiring thoughts and helpful suggestions for the project and the manuscript, and Dr. Lorenzo Finci (Peking University/Harvard Medical School) for his meticulous editing of the manuscript. We also thank Dr. Sisodia for providing the PS1 mutant mouse lines and Dr. Bennett for providing the AnkG constructs and antibody. This work was supported by the National Science Foundation of China (Major Research Grant 91132718) and the Beijing Natural Science Foundation (Grant 7142085).

1. Price DL, Sisodia SS, Gandy SE (1995) Amyloid beta amyloidosis in Alzheimer's disease. *Curr Opin Neurol* 8(4):268–274.
2. Bayer TA, et al. (2001) Key factors in Alzheimer's disease: Beta-amyloid precursor protein processing, metabolism and intraneuronal transport. *Brain Pathol* 11(1):1–11.
3. Wirths O, Weis J, Szczygielski J, Multhaup G, Bayer TA (2006) Axonopathy in an APP/PS1 transgenic mouse model of Alzheimer's disease. *Acta Neuropathol* 111(4):312–319.
4. Lagos-Quintana M, Rauhut R, Lendeckel W, Tuschl T (2001) Identification of novel genes coding for small expressed RNAs. *Science* 294(5543):853–858.
5. Jin P, et al. (2004) Biochemical and genetic interaction between the fragile X mental retardation protein and the microRNA pathway. *Nat Neurosci* 7(2):113–117.
6. Ashraf SI, McLoon AL, Sclarsic SM, Kunes S (2006) Synaptic protein synthesis associated with memory is regulated by the RISC pathway in *Drosophila*. *Cell* 124(1):191–205.
7. Elmén J, et al. (2008) LNA-mediated microRNA silencing in non-human primates. *Nature* 452(7189):896–899.
8. Hollander JA, et al. (2010) Striatal microRNA controls cocaine intake through CREB signalling. *Nature* 466(7303):197–202.
9. Chan AW, Kocerha J (2012) The path to microRNA therapeutics in psychiatric and neurodegenerative disorders. *Front Genet* 3:82.
10. Delay C, Mandemakers W, Hébert SS (2012) MicroRNAs in Alzheimer's disease. *Neurobiol Dis* 46(2):285–290.
11. Delay C, Hébert SS (2011) MicroRNAs and Alzheimer's disease mouse models: Current insights and future research avenues. *Int J Alzheimers Dis* 2011:894938.
12. Sun X, Wu Y, Gu M, Zhang Y (2014) miR-342-5p decreases ankyrin G levels in Alzheimer's disease transgenic mouse models. *Cell Reports* 6(2):264–270.
13. Peters L, Meister G (2007) Argonaute proteins: Mediators of RNA silencing. *Mol Cell* 26(5):611–623.
14. Eulalio A, et al. (2009) Deadenylation is a widespread effect of miRNA regulation. *RNA* 15(1):21–32.
15. Meister G (2007) miRNAs get an early start on translational silencing. *Cell* 131(1): 25–28.
16. Szu-Yu Ho T, Rasband MN (2011) Maintenance of neuronal polarity. *Dev Neurobiol* 71(6):474–482.
17. Rasband MN (2010) The axon initial segment and the maintenance of neuronal polarity. *Nat Rev Neurosci* 11(8):552–562.
18. Buffington SA, Rasband MN (2011) The axon initial segment in nervous system disease and injury. *Eur J Neurosci* 34(10):1609–1619.
19. Winckler B, Forscher P, Mellman I (1999) A diffusion barrier maintains distribution of membrane proteins in polarized neurons. *Nature* 397(6721):698–701.
20. Song AH, et al. (2009) A selective filter for cytoplasmic transport at the axon initial segment. *Cell* 136(6):1148–1160.
21. Kapfhamer D, et al. (1995) Chromosomal localization of the ankyrinG gene (ANK3/Ank3) to human 10q21 and mouse 10. *Genomics* 27(1):189–191.
22. Kordeli E, Lambert S, Bennett V (1995) AnkyrinG: A new ankyrin gene with neural-specific isoforms localized at the axonal initial segment and node of Ranvier. *J Biol Chem* 270(5):2352–2359.
23. Sobotzik JM, et al. (2009) AnkyrinG is required to maintain axo-dendritic polarity in vivo. *Proc Natl Acad Sci USA* 106(41):17564–17569.
24. Hedstrom KL, Ogawa Y, Rasband MN (2008) AnkyrinG is required for maintenance of the axon initial segment and neuronal polarity. *J Cell Biol* 183(4):635–640.
25. Mohler PJ, Gramolini AO, Bennett V (2002) The ankyrin-B C-terminal domain determines activity of ankyrin-B/G chimeras in rescue of abnormal inositol 1,4,5-trisphosphate and ryanodine receptor distribution in ankyrin-B (–/–) neonatal cardiomyocytes. *J Biol Chem* 277(12):10599–10607.
26. Hedstrom KL, et al. (2007) Neurofascin assembles a specialized extracellular matrix at the axon initial segment. *J Cell Biol* 178(5):875–886.
27. Yang Y, Ogawa Y, Hedstrom KL, Rasband MN (2007) betaIV spectrin is recruited to axon initial segments and nodes of Ranvier by ankyrinG. *J Cell Biol* 176(4):509–519.
28. Bréchet A, et al. (2008) Protein kinase CK2 contributes to the organization of sodium channels in axonal membranes by regulating their interactions with ankyrin G. *J Cell Biol* 183(6):1101–1114.
29. Zhou D, et al. (1998) AnkyrinG is required for clustering of voltage-gated Na channels at axon initial segments and for normal action potential firing. *J Cell Biol* 143(5): 1295–1304.
30. Hu W, et al. (2009) Distinct contributions of Na(v)1.6 and Na(v)1.2 in action potential initiation and backpropagation. *Nat Neurosci* 12(8):996–1002.
31. Setou M, Nakagawa T, Seog DH, Hirokawa N (2000) Kinesin superfamily motor protein KIF17 and mLin-10 in NMDA receptor-containing vesicle transport. *Science* 288(5472):1796–1802.
32. Guillaud L, Setou M, Hirokawa N (2003) KIF17 dynamics and regulation of NR2B trafficking in hippocampal neurons. *J Neurosci* 23(1):131–140.
33. Benshalom G, Reese TS (1985) Ultrastructural observations on the cytoarchitecture of axons processed by rapid-freezing and freeze-substitution. *J Neurocytol* 14(6):943–960.
34. Palay SL, Sotelo C, Peters A, Orkand PM (1968) The axon hillock and the initial segment. *J Cell Biol* 38(1):193–201.
35. Tóth ME, et al. (2013) Overexpression of Hsp27 ameliorates symptoms of Alzheimer's disease in APP/PS1 mice. *Cell Stress Chaperones* 18(6):759–771.
36. Kaczorowski CC, Sametsky E, Shah S, Vassar R, Disterhoft JF (2011) Mechanisms underlying basal and learning-related intrinsic excitability in a mouse model of Alzheimer's disease. *Neurobiol Aging* 32(8):1452–1465.
37. Yang Y, Cook DG (2004) Presenilin-1 deficiency impairs glutamate-evoked intracellular calcium responses in neurons. *Neuroscience* 124(3):501–505.
38. Stutzmann GE, Caccamo A, LaFerla FM, Parker I (2004) Dysregulated IP3 signaling in cortical neurons of knock-in mice expressing an Alzheimer's-linked mutation in presenilin1 results in exaggerated $Ca2^{+}$ signals and altered membrane excitability. *J Neurosci* 24(2):508–513.
39. Sepulveda-Falla D, et al. (2014) Familial Alzheimer's disease-associated presenilin-1 alters cerebellar activity and calcium homeostasis. *J Clin Invest* 124(4):1552–1567.
40. Abad MA, Enguita M, DeGregorio-Rocasolano N, Ferrer I, Trullas R (2006) Neuronal pentraxin 1 contributes to the neuronal damage evoked by amyloid-beta and is overexpressed in dystrophic neurites in Alzheimer's brain. *J Neurosci* 26(49):12735–12747.
41. Szapacs ME, Numis AL, Andrews AM (2004) Late onset loss of hippocampal 5-HT and NE is accompanied by increases in BDNF protein expression in mice co-expressing mutant APP and PS1. *Neurobiol Dis* 16(3):572–580.
42. Lazarov O, et al. (2007) Impairments in fast axonal transport and motor neuron deficits in transgenic mice expressing familial Alzheimer's disease-linked mutant presenilin 1. *J Neurosci* 27(26):7011–7020.
43. Magini A, et al. (2010) Fibroblasts from PS1 mutated pre-symptomatic subjects and Alzheimer's disease patients share a unique protein levels profile. *J Alzheimers Dis* 21(2):431–444.
44. Fleisher AS, et al. (2012) Florbetapir PET analysis of amyloid-β deposition in the presenilin 1 E280A autosomal dominant Alzheimer's disease kindred: A cross-sectional study. *Lancet Neurol* 11(12):1057–1065.
45. Cui J, et al. (2011) Morphine protects against intracellular amyloid toxicity by inducing estradiol release and up-regulation of Hsp70. *J Neurosci* 31(45):16227–16240.
46. Saito T, Nakatsuji N (2001) Efficient gene transfer into the embryonic mouse brain using in vivo electroporation. *Dev Biol* 240(1):237–246.